Inorganic Chemistry

Article

pubs.acs.org/IC

Water Oxidation Chemistry of a Synthetic Dinuclear Ruthenium Complex Containing Redox-Active Quinone Ligands

Hiroshi Isobe,*[,†,‡] Koji Tanaka,[§] Jian-Ren Shen,[†] and Kizashi Yamaguchi[‡,∥]

[†]Division of Bioscience, Graduate School of Natural Science and Technology/Faculty of Science, Okayama University, Okayama 700-8530, Japan

[‡]Department of Regulatory Bioorganic Chemistry, The Institute of Scientific and Industrial Research, Osaka University, Ibaraki, Osaka 567-0047, Japan

[§]Institute for Integrated Cell-Material Sciences, Kyoto University, Kyoto 615-8530, Japan

[∥]Institute for NanoScience Design, Osaka University, Toyonaka, Osaka 560-0043, Japan

Supporting Information

ABSTRACT: We investigated theoretically the catalytic mechanism of electrochemical water oxidation in aqueous solution by a dinuclear ruthenium complex containing redox-active quinone ligands, $[Ru_2(X)(Y)(3,6\text{-}tBu_2Q)_2(btpyan)]^{m+}$ [X, Y = H_2O, OH, O, O_2; 3,6-tBu_2Q = 3,6-di-*tert*-butyl-1,2-benzoquinone; btpyan =1,8-bis(2,2′:6′,2″-terpyrid-4′-yl)anthracene] (*m* = 2, 3, 4) (**1**). The reaction involves a series of electron and proton transfers to achieve redox leveling, with intervening chemical transformations in a mesh scheme, and the entire molecular structure and motion of the catalyst **1** work together to drive the catalytic cycle for water oxidation. Two substrate water molecules can bind to **1** with simultaneous loss of one or two proton(s), which allows pH-dependent variability in the proportion of substrate-bound structures and following pathways for oxidative activation of the aqua/hydroxo ligands at low thermodynamic and kinetic costs. The resulting bis-oxo intermediates then undergo endothermic O−O radical coupling between two Ru(III)−O$^{\bullet}$ units in an anti-coplanar conformation leading to bridged *μ*-peroxo or *μ*-superoxo intermediates. The *μ*-superoxo species can liberate oxygen with the necessity for the preceding binding of a water molecule, which is possible only after four-electron oxidation is completed. The magnitude of catalytic current would be limited by the inherent sluggishness of the hinge-like bending motion of the bridged *μ*-superoxo complex that opens up the compact, hydrophobic active site of the catalyst and thereby allows water entry under dynamic conditions. On the basis of a newly proposed mechanism, we rationalize the experimentally observed behavior of electrode kinetics with respect to potential and discuss what causes a high overpotential for water oxidation by **1**.

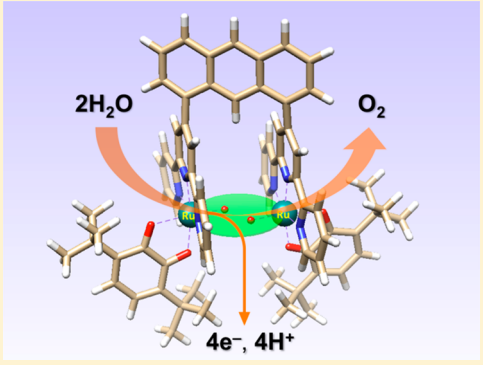

1. INTRODUCTION

With the urgent need to address energy and environmental concerns on our earth, there has been growing interest in developing technologies for producing, storing, and using energy without consumption of fossil fuels.[1] Use of solar photons to produce high-energy chemical bonds from water as a reducing agent that is always available and production of electrical energy by chemical reactions could supply clean and renewable energy sources.[1] The major obstacle that limits the efficiency achievable concerns oxidation of water to yield oxygen as a byproduct, one of the half reactions of water splitting, as shown in eq 1.

$$2H_2O \rightarrow O_2 + 4e^- + 4H^+ \quad E^\circ = 1.23\ \text{V vs SHE at pH} = 0 \tag{1}$$

This anodic reaction requires coupling of four electron and proton transfers from two water molecules and formation of an O−O bond, which make this reaction mechanistically complex and energetically demanding. The overall process must clearly involve several elementary reactions through four successive electron-transfer steps, as indicated in eqs 2−4.[2]

$$2H_2O \rightarrow H_2O + HO^{\bullet} + e^- + H^+ \quad E^\circ = 2.72\ \text{V} \tag{2}$$

$$2H_2O \rightarrow HOOH + 2e^- + 2H^+ \quad E^\circ = 1.76\ \text{V} \tag{3}$$

$$2H_2O \rightarrow HOO^{\bullet} + 3e^- + 3H^+ \quad E^\circ = 1.66\ \text{V} \tag{4}$$

The thermodynamic instability of free hydroxyl radical (HO$^{\bullet}$) results in the source of a substantial overpotential. To develop viable systems for water oxidation, it is necessary to incorporate rationally designed catalysts to be able to drive the reaction cycle at potentials as close as possible to the thermodynamic limit for the four-electron oxidation of water (E° = 1.23 V).[3] The long-term physical and chemical stabilities of the catalysts under oxidizing conditions are also of particular concern for practical applications.

Received: September 16, 2013
Published: April 2, 2014

   dx.doi.org/10.1021/ic402340d | *Inorg. Chem.* 2014, 53, 3973−3984

In nature, a remarkable molecular catalyst, the oxygen-evolving complex (OEC) buried in the enzyme photosystem II, performs this difficult reaction by storing redox equivalents in a cluster containing four manganese ions, one calcium ion, and five oxygen atoms (Mn_4CaO_5).[4−6] Although catalytic transformations in the OEC are not fully understood, this chemistry is essential for all aerobic life on our earth and has received a considerable amount of attention both for its biological significance and as a challenge for biomimetic modeling for artificial photosynthesis.[1,3−6] A lot of work has been devoted to the design and preparation of homogeneous and heterogeneous synthetic oxidation catalysts containing transition metals such as ruthenium (Ru),[7] iridium (Ir),[8] manganese (Mn),[9] cobalt (Co),[10] and iron (Fe)[11] ions that can emulate the efficiency of the OEC (close to the thermodynamic limit), but their catalytic activity and stability are still far from those of the OEC.

Ru-based complexes constitute a major class of synthetic molecular catalysts for water oxidation and have been most extensively studied.[7] The first well-characterized catalyst is a dinuclear Ru complex known also as the "blue dimer", *cis*,*cis*-$[(bpy)_2(H_2O)Ru(\mu\text{-}O)Ru(H_2O)(bpy)_2]^{4+}$ (bpy = 2,2′-bipyridine), synthesized by the Meyer group, which contains two Ru(III)−OH_2 groups bridged by an oxo ligand in a cis orientation.[12] In the presence of excess Ce(IV) ions, this catalyst showed oxygen evolution with at least 13.2 turnover cycles.[13] This intriguing catalytic system initiated development of oxo-bridged dinuclear Ru complexes, $[L(H_2O)Ru(\mu\text{-}O)Ru(H_2O)L]$ (L = nonbridging ligand), that mimic the blue dimer.[14] To improve the stability of the blue dimer types of complexes, which often suffer from oxidative degradation upon catalytic activity,[15] dinuclear Ru complexes bridged by rigid ligands, $[L(H_2O)Ru(\mu\text{-BL})Ru(H_2O)L]$ (μ-BL = bridging ligand), have also been prepared and shown to oxidize water to molecular oxygen.[16] Recently, a number of reports have appeared on mononuclear Ru and other transition-metal complexes, which become an important family of catalysts capable of oxidizing water at a single metal site.[17] The coincident emergence of polyoxometallate (POM)-based catalysts could also make a significant stage in the development of water oxidation catalysts.[3d,18]

To realize the full potential of synthetic catalysts, we must develop a profound understanding of catalytic mechanisms in both synthetic and biological systems. Comprehensive and thorough examinations can yield a rich variety of chemical information, which may serve as means to design effective catalysts. To gain insights into artificial water splitting, we decided to investigate theoretically the catalytic mechanism of water oxidation by a dinuclear Ru complex $[Ru_2(X)(Y)(3,6\text{-}tBu_2Q)_2(btpyan)]^{m+}$ [X, Y = H_2O, OH, O, O_2; 3,6-tBu_2Q = 3,6-di-*tert*-butyl-1,2-benzoquinone; btpyan =1,8-bis(2,2′:6′,2″-terpyrid-4′-yl)anthracene] (*m* = 2, 3, 4) (**1**, Chart 1),[19] which was designed and synthesized by Tanaka and co-workers.[20] A notable point of this dinuclear complex is that each Ru center is coordinated by a redox-active quinone ligand (3,6-tBu_2Q or simply Q). The rest of the distorted octahedral coordination positions are complexed by an anthracene-bridged bis-terpyridine ligand (btpyan), so that two $[Ru(OH)(3,6\text{-}tBu_2Q)]^+$ units are placed in a cofacial conformation suited for a direct O−O coupling. Central to this approach is the idea that the quinone ligand can accept one or two electron(s) from an aqua ligand, coupled with acid−base equilibrium, to give a semiquinone radical (SQ) or a catecholate dianion (Cat), thereby facilitating formation of a Ru−O$^\bullet$ radical species in a low oxidation state, as shown in Scheme 1.[21] The chemistry of complex **1** is unique in that storage of multiple redox equivalents at spatially separated sites from metal ions serves to avoid high-energy intermediates in the intermediary stage of four-electron oxidation of water. The catalyst **1** was quite stable toward degradation and executed catalytic function with a turnover number for O_2 evolution as high as 33 500 when deposited on an indium−tin oxide (ITO) electrode in water (pH = 4.0).[20b] Cyclic voltammetry (CV) analysis of **1** revealed that there is a reversible redox wave at a very low potential (0.32 V vs Ag/AgCl) that is followed by an irreversible anodic wave at a quite positive potential (1.19 V) and an appreciable catalytic current above 1.5 V.[20b]

Quantum chemical modeling using hybrid density functional theory (DFT) has recently been applied by two groups to the mechanistic investigations of water oxidation by a truncated model of **1**, in which *tert*-butyl groups on quinone ligands are replaced by hydrogens.[22,23] Their interpretations are partly inconsistent. Muckerman et al. surmised that four-proton loss from two molecules of water precedes four-electron oxidation, leading to formation of a superoxo bridge between two Ru(II) centers, $[(Q^{-1.5})Ru^{II}(\mu\text{-}OO^{\bullet-})Ru^{II}(Q^{-1.5})(btpyan)]^0$, as a key intermediate.[22] As an alternative for this spontaneous formation of an O−O bond, Ghosh and Baik proposed that alternating

Chart 1

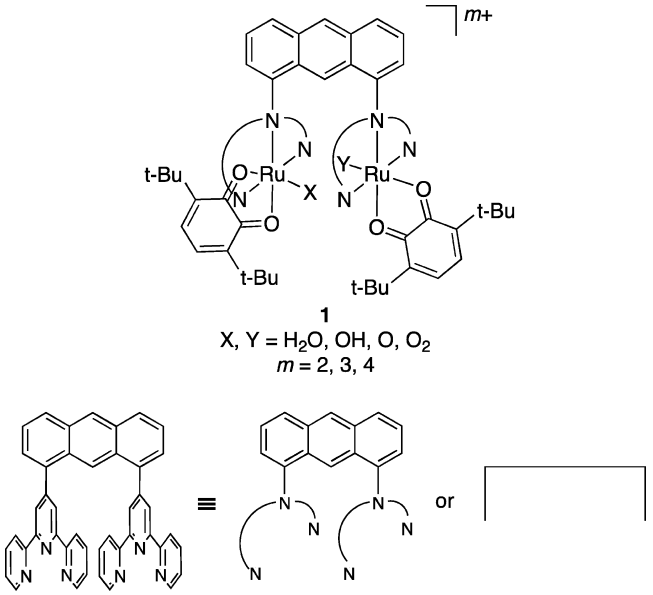

Scheme 1

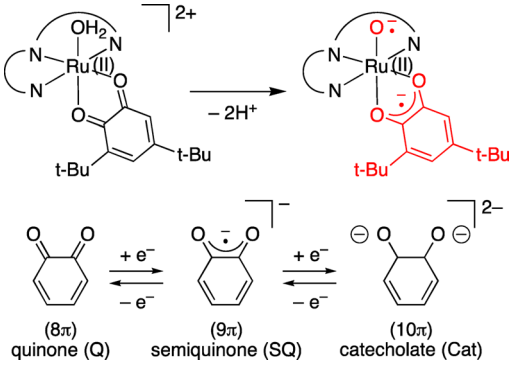

dx.doi.org/10.1021/ic402340d | Inorg. Chem. 2014, 53, 3973−3984

removal of two protons and two electrons occurs in water from an oxo−aqua complex, $^1[(SQ)Ru^{III}(O^{\bullet-})(H_2O)Ru^{II}(SQ)(btpyan)]^{2+}$, to give two Ru(III)−O$^\bullet$ fragments, $[(SQ)Ru^{III}(O^{\bullet-})(O^{\bullet-})Ru^{III}(SQ)(btpyan)]^{2+}$, which then undergo direct radical coupling with a significant barrier of 19.7 kcal mol^{-1}.[23] The experimentally observed single reversible wave at 0.32 V was suggested to arise from a two-electron overall electrochemical response.[23a] They further speculated that O−O bond formation could be followed with loss of a Ru−quinone bond and rearrangement to release a molecular oxygen and incorporate substrate water molecules.[23b]

In this study, our efforts to understand the overall catalytic cycle of water oxidation by the dinuclear Ru complex **1** are described using the B3LYP hybrid density functional. Thermodynamic and kinetic data obtained from a complete model of **1** provide different mechanistic features from those reported by previous studies;[22,23] multiple reaction pathways are apparent, and a large-amplitude structural change of the catalyst plays a role in catalytic activity. We will describe the detailed redox chemistry of **1** and discuss the reasons for the experimentally observed behavior of electrode kinetics with respect to potential, based on a newly proposed mechanism, to understand what causes a high overpotential for water oxidation by **1**.

2. COMPUTATIONAL DETAILS

To investigate the redox chemistry of the dinuclear ruthenium complex realistically, a full molecular catalyst of **1** was employed in the present study. Quantum-chemical calculations were performed with Gaussian 09.[24] Unless otherwise noted, all geometries were fully optimized in the gas phase using the B3LYP hybrid density functional[25] combined with the basis sets of double-ζ quality, Los Alamos LANL2DZ[26a] for the Ru atom and 6-31G(d)[26b] for all other atoms, which are abbreviated as BS1. Frequency calculations were carried out with BS1 to verify the nature of all stationary points and to derive zero-point energies without scaling and thermal contributions to Gibbs free energy at 298.15 K. The final energetics was further evaluated by single-point calculations at each optimized geometry with an extensive triple-ζ quality basis set augmented with polarization and diffuse functions on all atoms, LANL2TZ(f)[26c] for the Ru atom, and 6-311+G(2d,p)[26b] for all other atoms, henceforth designated as BS2. Polarity effect by the bulk solvent was evaluated by the conductor-like polarizable continuum model (CPCM)[27] at the B3LYP/BS2 level in combination with the cavity built by the united atom Kohn−Sham topological model (UAKS) implemented in Gaussian 09. The dielectric constant of 78.39 was used to represent the water solvent.

We evaluated the dissociation constant K_a or its negative logarithm pK_a of a redox intermediate, denoted here by HA, from the aqueous free-energy change of acid dissociation ΔG°_{sol} referenced to 1 M standard state, as shown in eqs 5 and 6, in which R is the gas constant and T temperature (298.15 K).

$$HA \rightarrow A^- + H^+ \quad \Delta G^\circ_{sol} \tag{5}$$

$$pK_a(HA) = \Delta G^\circ_{sol}/2.303RT \tag{6}$$

The ΔG°_{sol} value can be derived from a thermodynamic cycle, as given in eq 7, in which G°_{gas} is the gas-phase free energy referenced to 1 atm standard state and ΔG°_{solv} the solvation free energy referenced to 1 M gas and 1 M solution standard state plus free energy needed for transfer of a solute molecule from 1 atm gas to 1 M gas standard state [$RT\ln(24.46)$ = 1.89 kcal mol^{-1}].

$$\Delta G^\circ_{sol} = G^\circ_{gas}(A^-) + G^\circ_{gas}(H^+) - G^\circ_{gas}(HA) + \Delta G^\circ_{solv}(A^-) + \Delta G^\circ_{solv}(H^+) - \Delta G^\circ_{solv}(HA) \tag{7}$$

The free energy of gas-phase proton $G^\circ_{gas}(H^+)$ (−6.28 kcal mol^{-1}) and the solvation free energy of proton $\Delta G^\circ_{solv}(H^+)$ (−264.0 kcal mol^{-1}) are taken from the literature.[28,29]

The standard redox potential in aqueous solution E° was determined from a half reaction, as shown in eqs 8−10, in which ΔG°_{sol} is the free-energy change associated with the half reaction, F the Faraday constant (23.06 kcal mol^{-1} V^{-1}), and 4.43 V the absolute potential (i.e., vs a free electron in vacuum) of the standard hydrogen electrode (SHE).[30]

$$Ox(water) + e^-(vacuum) \rightarrow Red(water) \quad \Delta G^\circ_{sol} \tag{8}$$

$$E^\circ \text{ vs SHE} = -\Delta G^\circ_{sol}/F - 4.43 \text{ V} \tag{9}$$

$$\Delta G^\circ_{sol} = G^\circ_{gas}(Red) - G^\circ_{gas}(Ox) + \Delta G^\circ_{solv}(Red) - \Delta G^\circ_{solv}(Ox) \tag{10}$$

3. RESULTS

We present below the key results of the catalytic cycle of water oxidation by the dinuclear ruthenium (Ru) complex **1** in aqueous solution by separating three parts: (I) oxidative activation of two water molecules to give bis-oxo intermediates, (II) O−O bond formation to give bridged μ-peroxo or μ-superoxo intermediates, and (III) oxygen release and substrate water binding. In the following description of complexes, the btpyan ligand is omitted for clarity, unless it is involved as a redox-active ligand; *tert*-butyl substituents attached to the quinone (Q) and semiquinone (SQ) ligands are also omitted to simplify notation; and two Ru(Q)/Ru(SQ) units are distinguished by the subscripts L (left-hand side) and R (right-hand side). We sometimes call the complex simply the +2, +3, or +4 system by noting the total charge. Each Ru center is always assumed to be in a low-spin state, i.e., S_{Ru} = 0 and 1/2 for Ru(II)-d^6 and Ru(III)-d^5 sites. For convenience, integer formal oxidation numbers are assigned to Ru ions and ligands; however, we must be careful to remember that unpaired electrons may be delocalized whenever possible, so that the actual oxidation state may be somewhat different from the formal one. Mullken charge and spin densities for all structures reported in this paper are available as Supporting Information.

3.1. Oxidative Activation of Two Water Molecules.

Figure 1 summarizes the redox properties for oxidative activation of two water molecules by **1** leading to bis-oxo intermediates.[31] The results are in qualitative agreement with effective exchange integrals determined previously,[19] which predict that the SQ$^{\bullet-}$−Ru(III)$^\bullet$−OH$^-$, SQ$^{\bullet-}$−Ru(II)−O$^\bullet$, and Q−Ru(III)$^\bullet$−O$^\bullet$ units should have ↑↓, ↑↑, and ↑↑ spin arrangements in the ground state during water activation. In previous computational studies using a simplified model with *tert*-butyl groups on quinone ligands replaced by hydrogens[22,23] there is a difference between two groups in the assignment of the most reduced state of the substrate-bound complex, called below the resting state. Muckerman et al.[22] suggested that removal of two protons from two water substrates in $^1[(Q_L)Ru_L^{II}(H_2O)(H_2O)Ru_R^{II}(Q_R)]^{4+}$ in the gas phase leads to a bis-hydroxo complex, $^1[(Q_L)Ru_L^{II}(OH)(OH)Ru_R^{II}(Q_R)]^{2+}$, while in the study by Ghosh and Baik[23a] the doubly deprotonated species was assigned as an oxo−aqua complex, $^1[(SQ_L)Ru_L^{III}(O^{\bullet-})(H_2O)Ru_R^{II}(SQ_R)]^{2+}$, in aqueous solution. Our results, based on a full model, predict the lowest structure of the doubly deprotonated form of the resting state to be a bis-hydroxo complex with a formal oxidation state of III on each Ru ion, $^1[(SQ_L)Ru_L^{III}(OH)(OH)Ru_R^{III}(SQ_R)]^{2+}$, both in the gas phase and in aqueous solution, which lies 6.6 and 3.9 kcal

dx.doi.org/10.1021/ic402340d | Inorg. Chem. 2014, 53, 3973−3984

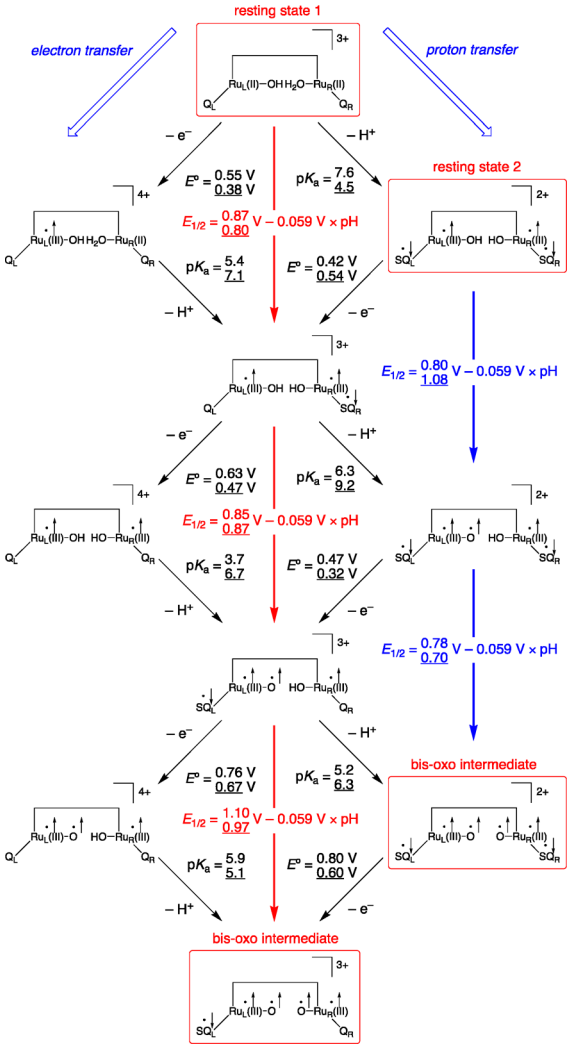

Figure 1. Thermodynamic results for oxidative activation of two water molecules by dinuclear Ru complex **1** in aqueous solution at the B3LYP/BS2//BS1 level by the CPCM-UAKS method; results based on solution-phase geometries are underlined.[31]

mol^{-1} below the oxo−aqua complex. Deprotonation of the two water ligands is expected to raise the energy level of electrons on each Ru center high enough to promote an electron into the lowest unoccupied molecular orbital of the quinone ligand, which is relatively low lying. As a result, the entire system acquires a tetraradical character with an antiferromagnetically coupled electron pair on each Ru(III)$^{\bullet}$−SQ$^{\bullet-}$ unit. Electron transfer between the Ru center and the ligand results in an electronic flexibility of the catalyst that arises from the presence of many low-lying isomers differing in charge, spin, and geometry (Tables S4−S6, Supporting Information).

The mechanism of water activation starting from $^{1}[(SQ_L)\text{-}Ru_L^{III}(OH)(OH)Ru_R^{III}(SQ_R)]^{2+}$, as indicated by two blue arrows in Figure 1, is in line with the one suggested by Ghosh and Baik,[23a] despite the inconsistency on the assignment of the resting state of the catalytic cycle. The bis-hydroxo complex and its activated species are coupled in an overall two-electron/two-proton ($2e^-/2H^+$) multiredox process, which comprises sequential proton-coupled electron transfer (PCET) to avoid charge accumulation.[32] Each PCET reaction is expected to proceed by electron loss from a semiquinone ligand followed by proton loss from a hydroxo ligand on the same side of the complex (ET-PT). A pathway that reverses the order [a proton transfer followed by an electron transfer (PT-ET)] is prohibited by very high pK_a values of 20−32 units for the initial proton-transfer step (Figure S1, Supporting Information). Successive deprotonations are also progressively less favorable. Once an unpaired electron on the semiquinone ligand (SQ) is transferred to the electrode, the resulting quinone ligand (Q) reacquires another electron from a substrate ligand (OH), triggered by proton loss from OH in an acid−base reaction, to return to the semiquinone radical in preparation for a later interfacial electron transfer. One PCET process creates an oxy radical, and the same event repeats once again on the other side. As a result, a bis-oxo hexaradical intermediate, $^{3}[(SQ_L)Ru_L^{III}(O^{\bullet-})(O^{\bullet-})Ru_R^{III}(SQ_R)]^{2+}$, is formed as a key active species. The redox potentials for the two PCET reactions are very low (0.7−1.1 V vs SHE at pH = 0). These results indicate the important role of redox-active quinone ligands in modulating redox potentials at a relatively

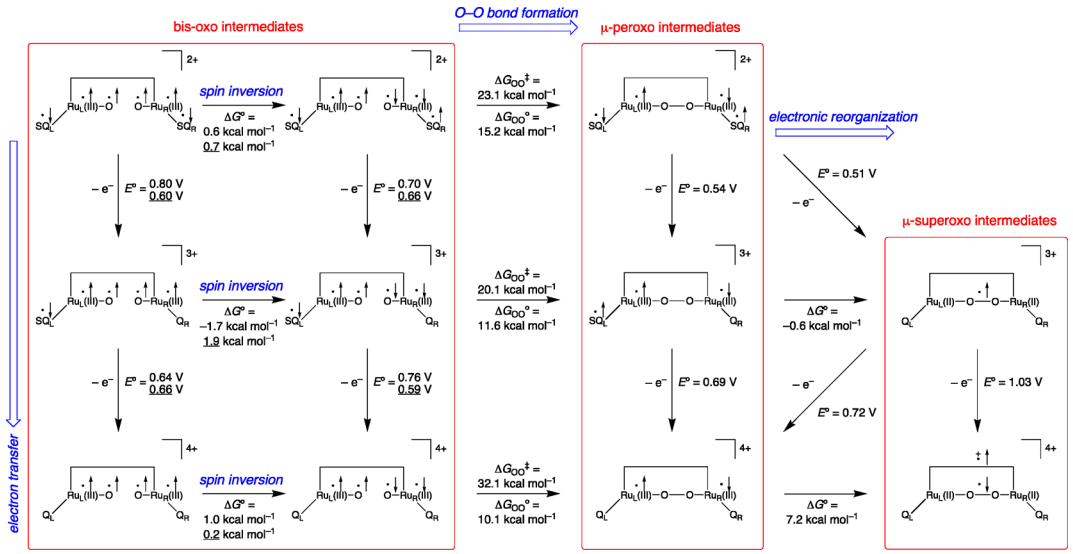

Figure 2. Thermodynamic results for O−O bond formation by dinuclear Ru complex **1** in aqueous solution at the B3LYP/BS2//BS1 level by the CPCM-UAKS method; results based on solution-phase geometries are underlined.[31]

dx.doi.org/10.1021/ic402340d | Inorg. Chem. 2014, 53, 3973−3984

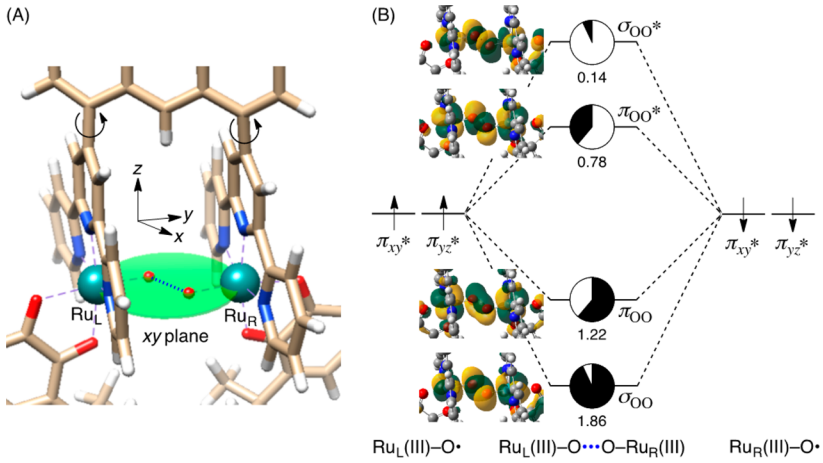

Figure 3. (A) Transition structure for O−O bond formation in $^{2}[(SQ_L)Ru_L^{III}(O^{\bullet-})(O^{\bullet-})Ru_R^{III}(Q_R)]^{3+}$ optimized at the B3LYP/BS1 level; (B) natural orbitals and their occupation numbers for σ and π interactions between two Ru(III)−O$^{\bullet}$ units.

low level by storing multiple redox equivalents at spatially separated sites in the intermediary stage of multielectron/multiproton oxidation.[22,23]

There can be another series of PCET processes for water activation, as indicated by the three red arrows in Figure 1, which is not addressed in the previous studies. This series starts with a singly deprotonated form of the resting state with a total charge of +3, $^{1}[(Q_L)Ru_L^{II}(OH)(H_2O)Ru_R^{II}(Q_R)]^{3+}$, and might progress in a mild acidic condition by an overall three-electron/three-proton ($3e^{-}/3H^{+}$) process leading to $^{4}[(SQ_L)Ru_L^{III}(O^{\bullet-})(O^{\bullet-})Ru_R^{III}(Q_R)]^{3+}$ or by an overall two-electron/three-proton ($2e^{-}/3H^{+}$) process to give $^{3}[(SQ_L)Ru_L^{III}(O^{\bullet-})(O^{\bullet-})Ru_R^{III}(SQ_R)]^{2+}$. These results imply that the catalyst **1** has different water activation pathways that can be altered by the proton activity. At an acidic pH region ($\lesssim$5) the +3 charge series originating from $^{1}[(Q_L)Ru_L^{II}(OH)(H_2O)Ru_R^{II}(Q_R)]^{3+}$ will dominate the behavior, while increasing the pH quantity results in an increased contribution of the +2 charge series from $^{1}[(SQ_L)Ru_L^{III}(OH)(OH)Ru_R^{III}(SQ_R)]^{2+}$ and will approach the +2/+3 hybrid character. Such a pH dependence of decoupled electron- and proton-transfer pathways could lead to the existence of an optimal pH in terms of thermodynamic overpotential.[33] Henceforth, the singly deprotonated form of the resting state $^{1}[(Q_L)Ru_L^{II}(OH)(H_2O)Ru_R^{II}(Q_R)]^{3+}$ is called resting state 1, while the doubly deprotonated forms $^{1}[(SQ_L)Ru_L^{III}(OH)(OH)Ru_R^{III}(SQ_R)]^{2+}$ and $^{1}[(SQ_L)Ru_L^{III}(O^{\bullet-})(H_2O)Ru_R^{II}(SQ_R)]^{2+}$ are designated as resting states 2 and 2′. An intriguing point is that resting state 1 has a closed-shell configuration with two Ru(II)−Q units at the B3LYP level, while in resting states 2 and 2′ charge transfer occurs from the Ru center to the quinone ligand, leading to an open-shell radical character with two Ru(III)$^{\bullet}$−SQ$^{\bullet-}$ units. Note, however, that application of a wide variety of density functionals to the electronic structure of resting state 1 yields singlet diradical character corresponding to Q_L−Ru_L(II)−OH^{-} ↔ $SQ_L^{\bullet-}$−Ru_L(III)$^{\bullet}$−OH^{-} that is highly sensitive to the weight of the Hartree−Fock exchange [ranging from 0% (pure DFT) to 62% (M06-HF)], as shown in Table S7, Supporting Information.

3.2. O−O Bond Formation. Figure 2 summarizes thermodynamic results for O−O bond formation by dinuclear Ru catalyst **1**. Since formation of the bis-oxo intermediate, $^{3}[(SQ_L)Ru_L^{III}(O^{\bullet-})(O^{\bullet-})Ru^{III}(SQ)]^{2+}$, by two-electron oxidation is attended by double electron shift from two Ru−O moieties to two quinone ligands, this species already stores four oxidation equivalents at the two Ru(III)−O$^{\bullet}$ units required to make a O−O bond. Two electrons residing in two semiquinone ligands of $^{3}[(SQ_L)Ru_L^{III}(O^{\bullet-})(O^{\bullet-})Ru_R^{III}(SQ_R)]^{2+}$ can be further removed at relatively low potentials of 0.60−0.66 V vs SHE, while the redox character of the spatially separated Ru−O units remain unaffected. Consequently, there are three bis-oxo intermediates that can contribute to O−O bond formation:[34] $^{3}[(SQ_L)Ru_L^{III}(O^{\bullet-})(O^{\bullet-})Ru_R^{III}(SQ_R)]^{2+}$, $^{4}[(SQ_L)Ru_L^{III}(O^{\bullet-})(O^{\bullet-})Ru_R^{III}(Q_R)]^{3+}$, and $^{5}[(Q_L)Ru_L^{III}(O^{\bullet-})(O^{\bullet-})Ru_R^{III}(Q_R)]^{4+}$. All these species appear in two adjacent spin states that exhibit ferro- and antiferromagnetic exchange coupling between the two $[Ru^{III}(O^{\bullet-})(SQ)]^{+}/[Ru^{III}(O^{\bullet-})(Q)]^{2+}$ units: triplet and singlet for the +2 system, quartet and doublet for the +3 system, and quintet and singlet for the +4 system. The spins of electron pairs are very important in bond formation, which is only allowed for the antiparallel spin component. Spin inversion from the ferro- to the antiferromagnetic state, therefore, must precede O−O bond making, as shown in Figure 2.

We could locate three transition structures for O−O bond formation (TS_{OO}) nascent from the antiferromagnetic (singlet, doublet, and singlet) states of the +2, +3, and +4 systems that lead to bridged peroxo intermediates, $^{1}[(SQ_L)Ru_L^{III}(\mu\text{-}OO^{2-})Ru_R^{III}(SQ_R)]^{2+}$, $^{2}[(SQ_L)Ru_L^{III}(\mu\text{-}OO^{2-})Ru_R^{III}(Q_R)]^{3+}$, and $^{1}[(Q_L)Ru_L^{III}(\mu\text{-}OO^{2-})Ru_R^{III}(Q_R)]^{4+}$. All transition structures involve an anti-coplanar Ru_L−O···O−Ru_R conformation, as shown by a *xy* plane in Figure 3A, with O−O bond lengths of 1.856, 1.838, and 1.820 Å for the +2, +3, and +4 systems. This planar conformation serves to maximize simultaneously σ and π radical coupling between the two terminal oxo groups, both of which can be established by the overlap between the singly occupied π^{*} orbitals of the Ru(III)−O$^{\bullet}$ bonds. Natural orbital analysis for TS_{OO} in the +3 system, as depicted in Figure 3B, indeed indicates strong O−O σ bonding ($\langle\pi^{*}_{xy}(Ru_LO|\pi^{*}_{xy}(Ru_RO)\rangle$ = 0.86) and moderate O−O π bonding ($\langle\pi^{*}_{yz}(Ru_LO|\pi^{*}_{yz}(Ru_RO)\rangle$ = 0.22); similar trends are also observed for the +2 and +4 systems (Figures S5−S7, Supporting Information). Like the case with resting state 1, the choice of density functionals affects significantly the multireference character and activation energies of TS_{OO} (Table S8, Supporting Information). This indicates that multiconfigurational electronic structure calculations are inevitable in the

dx.doi.org/10.1021/ic402340d | *Inorg. Chem.* 2014, 53, 3973−3984

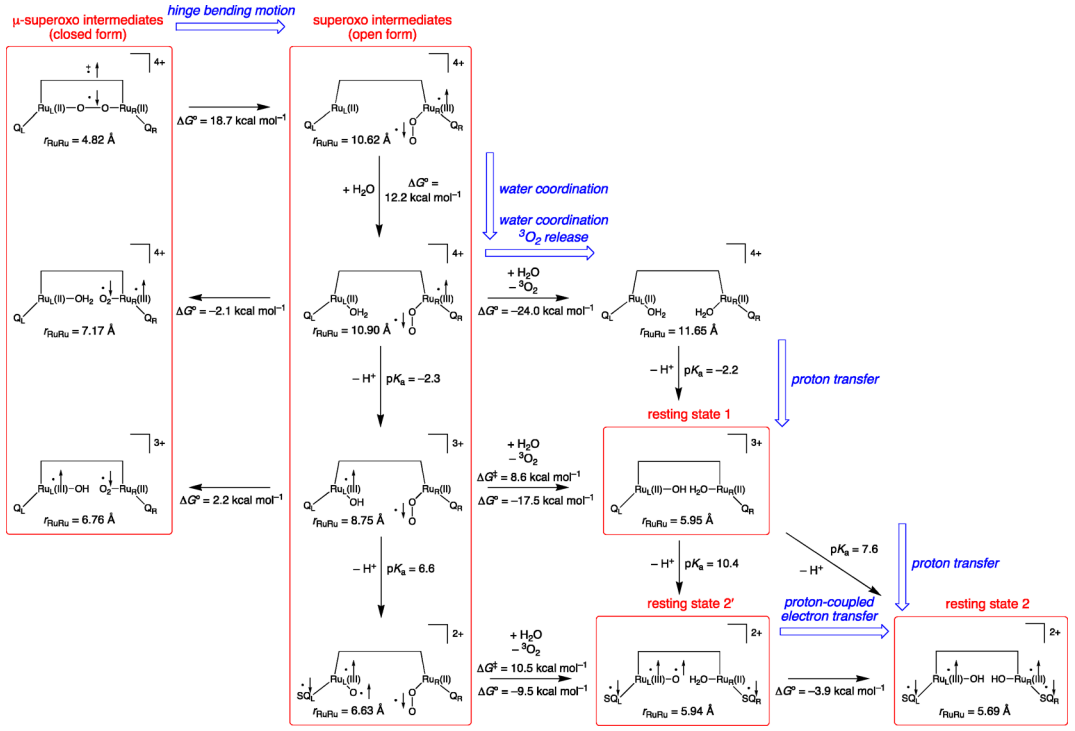

Figure 4. Thermodynamic results for oxygen release and substrate water binding by dinuclear Ru complex **1** in aqueous solution at the B3LYP/BS2//BS1 level by the CPCM-UAKS method.

proper description of TS_{OO} as well as resting state 1. Catalyst **1** is designed to have a flexibility related to the rotation about the C−C bond connecting the anthracene and tpy moieties, as indicated by two arrow-headed circles in Figure 3A, to adopt a geometry appropriate for O−O coupling.[23b]

The free energies of activation for the +2, +3, and +4 systems are calculated to be 20.2, 21.5, and 36.5 kcal mol^{-1} in the gas phase and 23.1, 20.1, 32.1 kcal mol^{-1} in aqueous solution. Although the activation energies for the +2 and +3 systems (20−22 kcal mol^{-1}) are available at room temperature, the barrier of 32.1 kcal mol^{-1} for the +4 system cannot be overcome thermally. The sluggish reactivity of Ru(III)−O$^{\bullet}$, as compared with high-valent Ru(V)═O (or Ru(IV)−O$^{\bullet}$), is also manifested by large endothermicities of about 10−15 kcal mol^{-1}. In the gas phase, two μ-peroxo intermediates, $^2[(SQ_L)Ru_L^{III}(\mu\text{-}OO^{2-})Ru_R^{III}(Q_R)]^{3+}$ and $^1[(Q_L)Ru_L^{III}(\mu\text{-}OO^{2-})Ru_R^{III}(Q_R)]^{4+}$, which are immediate products of the O−O coupling in the +3 and +4 systems, can then undergo electronic reorganization into μ-superoxo intermediates, $^2[(Q_L)Ru_L^{II}(\mu\text{-}OO^{\bullet-})Ru_R^{II}(Q_R)]^{3+}$ and $^1[(Q_L)Ru_L^{II}(\mu\text{-}OO^{\bullet-})Ru_R^{II}(Q_R)(btpyan^{\bullet+})]^{4+}$, which lie 5.5 and 1.3 kcal mol^{-1} below the μ-peroxo intermediates (Figure S4, Supporting Information). The increased electrophilicity of the Ru(III) site in the μ-superoxo complex is manifested in the fact that the semiquinone ligand transfers an electron to the Ru(III) site in the +3 system, while in the +4 system where there is no electron available in the quinone ligands the anthracene moiety replaces the role as an electron donor and is converted into an anthracene π-cation radical. The relative stabilities between μ-peroxo and μ-superoxo intermediates, however, exhibit very large solvent polarity dependence. The much better solvation of the μ-peroxo intermediates, $^2[(SQ_L)Ru_L^{III}(\mu\text{-}OO^{2-})Ru_R^{III}(Q_R)]^{3+}$ and $^1[(Q_L)Ru_L^{III}(\mu\text{-}OO^{2-})Ru_R^{III}(Q_R)]^{4+}$, makes the μ-peroxo → μ-superoxo conversion in aqueous solution nearly thermoneutral (−0.6 kcal mol^{-1}) for the +3 system and largely endothermic (7.2 kcal mol^{-1}) for the +4 system, as shown in Figure 2. These trends qualitatively follow the relative dipole moments: 19.0, 17.5, 12.7, and 10.1 D for $^2[(SQ_L)Ru_L^{III}(\mu\text{-}OO^{2-})Ru_R^{III}(Q_R)]^{3+}$, $^1[(Q_L)Ru_L^{III}(\mu\text{-}OO^{2-})Ru_R^{III}(Q_R)]^{4+}$, $^2[(Q_L)Ru_L^{II}(\mu\text{-}OO^{\bullet-})Ru_R^{II}(Q_R)]^{3+}$, and $^1[(Q_L)Ru_L^{II}(\mu\text{-}OO^{\bullet-})Ru_R^{II}(Q_R)(btpyan^{\bullet+})]^{4+}$.

3.3. Oxygen Release and Substrate Water Binding. To restart the catalyst, water substrates should replace the O_2 product in a ligand substitution concurrently with a change in the oxidation state of the Ru dimer from the most oxidized state to the most reduced state. We now consider how the catalyst liberates triplet O_2 from the three bridged superoxo complexes, $^1[(SQ_L)Ru_L^{II}(\mu\text{-}OO^{\bullet-})Ru_R^{III}(SQ_R)]^{2+}$, $^2[(Q_L)Ru_L^{II}(\mu\text{-}OO^{\bullet-})Ru_R^{II}(Q_R)]^{3+}$, and $^1[(Q_L)Ru_L^{II}(\mu\text{-}OO^{\bullet-})Ru_R^{II}(Q_R)(btpyan^{\bullet+})]^{4+}$, and recovers the resting state by binding two more water molecules. The resolution of the mechanism is a formidable challenge, since this process involves a large structural change of the catalyst, as shown later, which complicates the picture. The modeling of solvent water environment by an isotropic dielectric continuum is obviously oversimplified in that the solvent molecules would also make a significant entropy contribution to the free-energy change upon the structural change. Ghosh and Baik suggested that the most viable pathway involves initial addition of a water molecule from the bulk to one Ru(II) center, which replaces a Ru−quinone bond with a barrier of 25.6 kcal mol^{-1};[23b] however, analysis of a subsequent Ru−O bond breaking followed by release of a triplet O_2 has not been completed. Dissociation of a Ru−quinone bond more than once per cycle could cause rapid ligand degradation of the catalyst, which is inconsistent with the experimental fact that the dinuclear complex **1** is quite stable during the catalytic reaction.[20b]

dx.doi.org/10.1021/ic402340d | Inorg. Chem. 2014, 53, 3973−3984

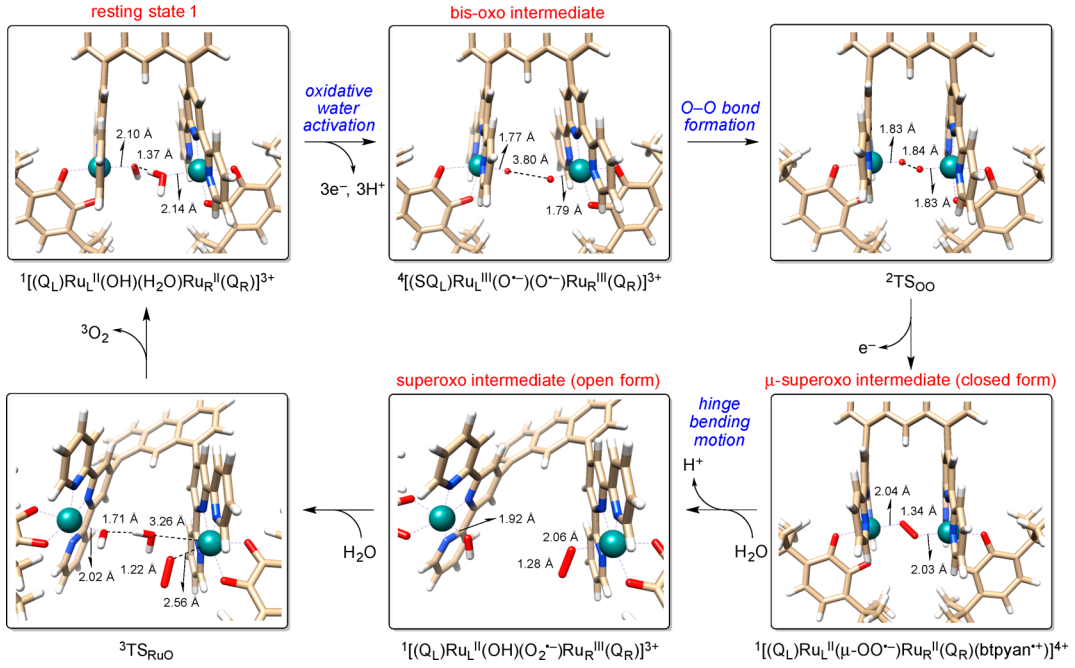

Figure 5. Geometrical parameters of several intermediates and transition structures for the catalytic cycle of water oxidation by dinuclear Ru complex **1** in acidic aqueous solutions at the B3LYP/BS1 level.

To find an alternative to this mechanism we simply considered that a large hinge-like bending motion of the μ-superoxo-bridged complex is essential for oxygen release and binding of substrate water molecules, since there is steric crowding within the cavity for water to substitute the μ-superoxo ligand. We scanned the potential surfaces of several low-lying states for the bending motion starting from the above three μ-superoxo complexes at the B3LYP/BS1 (or CAM-B3LYP) level by freezing the $Ru_L\cdots Ru_R$ internuclear distance (r_{RuRu}) and optimizing all other internal coordinates in the gas phase (Figure S8, Supporting Information). In the +2 and +3 systems, there is a steep rise in the potential curve (Figure S8A–D, Supporting Information). The energy continues to rise even at long $Ru_L\cdots Ru_R$ distances and never descends, which features a strongly bound superoxo anion $O_2^{\bullet-}$ (or a peroxo dianion O_2^{2-}) that serves as a ligand bridge to the two Ru ions. It will not be possible for the +2 and +3 systems to cleave a Ru–O bond by the hinge bending motion. In contrast, there is a flat region of potential surface in the +4 system, which lies after the lengthening of the $Ru_L\cdots Ru_R$ distance by more than about 1.7 Å (Figure S8E–G, Supporting Information). In this region, the energy level becomes steady at about 23 and 25 kcal mol^{-1} relative to the equilibrium state of $^1[(Q_L)Ru_L^{II}(\mu\text{-}OO^{\bullet-})Ru_R^{II}(Q_R)(btpyan^{\bullet+})]^{4+}$ for the singlet and triplet states. This flat region confers a flexibility of the catalyst enough to open its compact, hydrophobic active site and hence is apparently essential for O_2 evolution from the μ-superoxo species. What distinguishes this highly oxidized state from the lower oxidation states is that the anthracene moiety is oxidized to an electron-deficient cation radical, which can accept an electron from either $Ru_R(II)$ or a μ-superoxo bond ($OO^{\bullet-}$) as a Ru–O bond cleaves. This long-range electron transfer can be characterized by an intersection between two diabatic electronic states $^1[(Q_L)Ru_L^{II}(\mu\text{-}OO^{\bullet-})Ru_R^{II}(Q_R)(btpyan^{\bullet+})]^{4+}$ and $^1[(Q_L)Ru_L^{II}(O_2^{\bullet-})Ru_R^{III}(Q_R)]^{4+}$ (or $^3[(Q_L)Ru_L^{II}(^3O_2)Ru_R^{II}(Q_R)]^{4+}$) along the bending mode (Figure S8F,G, Supporting Information).[35]

On the basis of the above results, we can outline a mechanism for oxygen release and substrate binding, as shown in Figure 4, in which the closed and open forms of the superoxo complex are distinguished according to the $Ru_L\cdots Ru_R$ distance (r_{RuRu}). The open form with a long $Ru_L\cdots Ru_R$ distance can be reached only after four-electron oxidation is completed. This is the case for the +4 system, $^1[(Q_L)Ru_L^{II}(\mu\text{-}OO^{\bullet-})Ru_R^{II}(Q_R)(btpyan^{\bullet+})]^{4+}$ (or more stable $^1[(Q_L)Ru_L^{III}(\mu\text{-}OO^{2-})Ru_R^{III}(Q_R)]^{4+}$), which features a facile hinge-like movement at long $Ru_L\cdots Ru_R$ distances, as indicated in Figure S8E–G, Supporting Information, to enable effective catalysis. In contrast, +2 and +3 systems lock the catalyst in the closed form and thus are dead-end complexes that cannot evolve O_2, as shown in Figure S8A–D, Supporting Information. Although only the results for the singlet state are presented in Figure 4, we should be aware that there is always a closely lying triplet counterpart in the ground state (Figure S9, Supporting Information). Elongation of the $Ru_L\cdots Ru_R$ distance in the μ-superoxo complex $^1[(Q_L)Ru_L^{II}(\mu\text{-}OO^{\bullet-})Ru_R^{II}(Q_R)(btpyan^{\bullet+})]^{4+}$ gives rise to cleavage of the Ru_L–O bond, with an accompanying intramolecular electron transfer from $Ru_R(II)$ to $btpyan^{\bullet+}$, to produce the corresponding open conformation of the superoxo complex, $^1[(Q_L)Ru_L^{II}(O_2^{\bullet-})Ru_R^{III}(Q_R)]^{4+}$. The negative charge on $O_2^{\bullet-}$ makes it easier to oxidize the binding site, Ru_R. Once there is an electron transfer, a very small energy is sufficient enough to propagate the hinge bending motion, as we have seen above, to an extent that allows solvent water to penetrate the hydrophobic region. The endothermicity of this hinge bending process amounts to 18.7 kcal mol^{-1}; note, however, that this value does not include explicitly a large entropic loss in solvent, which originates from disruption of highly dynamic hydrogen-bonding network (the catalyst **1** is actually not soluble in water). In the open form $^1[(Q_L)Ru_L^{II}(O_2^{\bullet-})Ru_R^{III}(Q_R)]^{4+}$, the Ru_L–O bond is sufficiently long (>7 Å) to coordinate a water molecule at the coordinatively unsaturated $Ru_L(II)$ center. This water coordination process, $^1[(Q_L)Ru_L^{II}(O_2^{\bullet-})Ru_R^{III}(Q_R)]^{4+} + H_2O \rightarrow {}^1[(Q_L)Ru_L^{II}(H_2O)$-

dx.doi.org/10.1021/ic402340d | Inorg. Chem. 2014, 53, 3973–3984

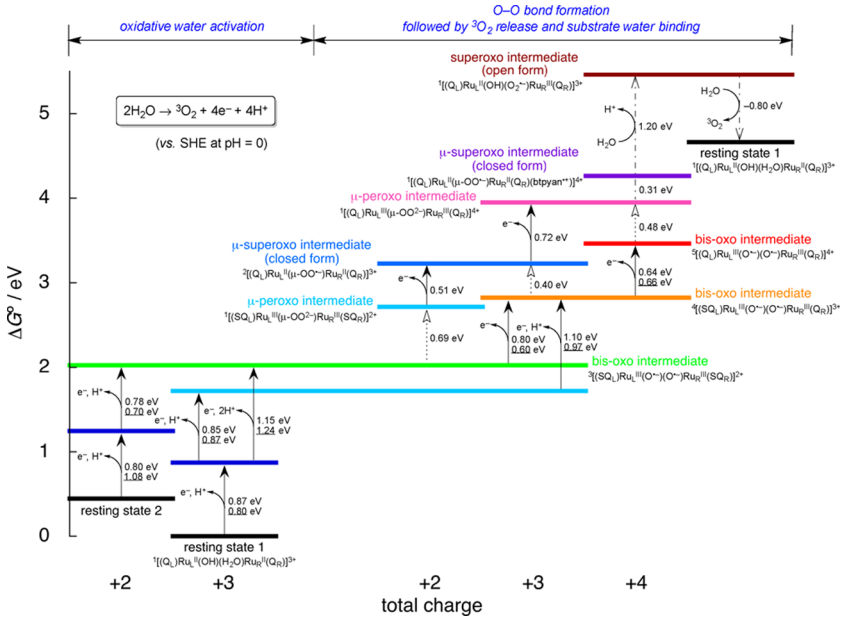

Figure 6. Energy diagram for the catalytic cycle of water oxidation by dinuclear Ru complex **1** in aqueous solution at pH = 0 with reference to SHE at the B3LYP/BS2//BS1 level by the CPCM-UAKS method; results based on solution-phase geometries are marked by underlines.[31]

$(O_2^{\bullet-})Ru_R^{III}(Q_R)]^{4+}$, is estimated to be endothermic by 12.2 kcal mol^{-1}. However, since the water molecule acquires increased acidity (pK_a = −2.3) once bound to the Ru_L site it will spontaneously lose a proton to the bulk, accompanied by a $Ru_L \rightarrow Ru_R$ electron shift, to form a hydroxo complex, $^1[(Q_L)Ru_L^{III}(OH)(O_2^{\bullet-})Ru_R^{II}(Q_R)]^{3+}$. The combination of these processes (water coordination and PCET processes) leads to an effectively concerted process that avoids the high-energy intermediates of the sequential mechanism, $^1[(Q_L)\text{-}Ru_L^{II}(O_2^{\bullet-})Ru_R^{III}(Q_R)]^{4+} + H_2O \rightarrow {}^1[(Q_L)Ru_L^{III}(OH)(O_2^{\bullet-})\text{-}Ru_R^{II}(Q_R)]^{4+} + H^+$, with an endothermicity that is not too large (pK_a = 6.6). The open and closed forms may be interconvertible with a free-energy change of about 2 kcal mol^{-1} (an entropic contribution in the solvent neglected), as shown in Figure 4.

In acidic aqueous solutions (pH $\lesssim$ 7), the open conformer of the $^1[(Q_L)Ru_L^{III}(OH)(O_2^{\bullet-})Ru_R^{II}(Q_R)]^{4+}$ complex is presumed to be implicated in release of a molecular oxygen from the catalyst. Dissociation of a triplet O_2 requires a spin inversion from the singlet to triplet state. Unlike the bis-oxo intermediates, the pair of the hydroxo−superoxo intermediates, $^{1,3}[(Q_L)Ru_L^{III}(OH)(O_2^{\bullet-})Ru_R^{II}(Q_R)]^{4+}$, will involve a fast precursor equilibrium between two adjacent singlet and triplet states, since a significant one-center integral of the orbital angular momentum operator between the mutually perpendicular π^* orbitals on $O_2^{\bullet-}$ causes a strong coupling between the two nearly degenerate spin states.[36] This fast pre-equilibrium spin isomerization will be followed by nucleophilic attack of a water molecule on the Ru_R center of the complex, which triggers an electron transfer from $O_2^{\bullet-}$ to the Ru_L(III) site. The Curtin−Hammett principle can be applied to this process, leading to O_2 dissociation predominantly on the lower-lying triplet surface. We could determine transition structures for the nucleophilic substitution reactions (TS_{RuO}) both on the singlet and on the triplet surfaces, which exhibit activation free energies of 10.0 and 6.2 kcal mol^{-1} in the gas phase and 8.6 and 8.0 kcal mol^{-1} in aqueous solution. Replacement of $O_2^{\bullet-}$ with a nucleophile such as H_2O or OH^- is important to drive the liberation of a triplet O_2, since the potential surface along the dissociation of O_2 becomes an uphill slope, if there is no nucleophile near the Ru center. The system returns to $^1[(Q_L)\text{-}Ru_L^{II}(OH)(H_2O)Ru_R^{II}(Q_R)]^{3+}$ (resting state 1) and is now ready for the next cycle for water oxidation. In Figure 5, we display graphics of several intermediates and transition structures (TS_{OO} and TS_{Ruo}) for the catalytic cycle of water oxidation by **1** in acidic pHs along with optimized geometrical parameters.

One can think of the precursor singlet−triplet equilibrium state as a pair of the oxo−superoxo species, $^{1,3}[(SQ_L)\text{-}Ru_L^{III}(O^{\bullet-})(O_2^{\bullet-})Ru_R^{II}(Q_R)]^{4+}$, if the catalyzed reaction takes place at basic pHs (pH $\gtrsim$ 7). This precursor state can evolve a triplet O_2 by attack of a water molecule on the Ru_R center with activation barriers of 11.1 and 10.9 kcal mol^{-1} in the gas phase and 11.1 and 11.3 kcal mol^{-1} in aqueous solution for the singlet and triplet states. In this case the system recovers as a resting state the bis-hydroxo species, $^1[(SQ_L)Ru_L^{III}(OH)(OH)\text{-}Ru_R^{III}(SQ_R)]^{2+}$ (resting state 2), since the immediate oxo−aqua product $^1[(SQ_L)Ru_L^{III}(O^{\bullet-})(H_2O)Ru_R^{II}(SQ_R)]^{2+}$ (resting state 2′) is unstable and likely converts by a PCET reaction to the lower lying resting state 2 at thermal equilibrium, as shown in Figure 4.

4. DISCUSSION

The present study explores the catalytic mechanism of electrochemical water oxidation by a dinuclear ruthenium complex **1**. Figure 6 summarizes the computed energy diagram for the entire catalytic cycle in aqueous solution at pH = 0 with reference to SHE. This diagram is somewhat simplified; processes for spin inversion and electronic reorganization involving small energy changes are not shown explicitly for clarity. The free energy required for one turnover of the catalytic cycle is calculated to be 4.66 eV, which is 0.26 eV (6.0 kcal mol^{-1}) smaller than the experimental value (4.92 eV). The fact that the theoretical and experimental values differ only by about 5% means that large entropy loss and gain in the water solvent upon dynamic opening and closing hinge bending

dx.doi.org/10.1021/ic402340d | Inorg. Chem. 2014, 53, 3973−3984

motions, which cannot be addressed explicitly by the PCM model, might be similar in magnitude and tend to cancel.

The cyclic voltammogram of the dinulear Ru catalyst **1** modified on an ITO electrode in water at pH = 4 showed (i) a broad reversible redox wave centered at 0.32 V vs Ag/AgCl, (ii) an irreversible anodic wave at 1.19 V, and (iii) a strong catalytic current above 1.5 V. We attempt to rationalize qualitatively the observed behavior of electrode kinetics with respect to potential for water oxidation by **1** with plausible reasons. To facilitate a comparison with the CV result, the energy diagram at pH = 4 relative to Ag/AgCl is also presented in Figure S10, Supporting Information. The information in Figures 6 and S10, Supporting Information, will serve as the basis for the following discussion.

Ghosh and Baik suggested that the first two PCET reactions give rise to a single two-electron wave response in the CV experiment.[23a] In accordance with their suggestion, the present calculations show that the initial two-electron oxidation reactions for water activation all fit into the narrow potential range (0.70−1.08 V vs SHE at pH = 0) in both the +2 and the +3 systems, as shown in Figure 6, except for an $e^-/2H^+$ process in the +3 system, which requires a higher potential of 1.24 V because of the loss of two protons. By extrapolating the potentials to pH = 4 and converting the reference electrode from SHE to Ag/AgCl, however, all e^-/H^+ and $e^-/2H^+$ potentials in the +2 and +3 systems are jammed within the range of 0.27−0.65 V vs Ag/AgCl at pH = 4 (Figure S10, Supporting Information). In addition, one-electron removal from the semiquinone ligand in bis-oxo intermediates $^3[(SQ_L)Ru_L^{III}(O^{\bullet-})(O^{\bullet-})Ru_R^{III}(SQ_R)]^{2+}$, $^1[(SQ_L)Ru_L^{III}(O^{\bullet-})(O^{\bullet-})Ru_R^{III}(SQ_R)]^{2+}$, $^4[(SQ_L)Ru_L^{III}(O^{\bullet-})(O^{\bullet-})Ru_R^{III}(Q_R)]^{3+}$, and $^2[(SQ_L)Ru_L^{III}(O^{\bullet-})(O^{\bullet-})Ru_R^{III}(Q_R)]^{3+}$ (0.40, 0.46, 0.46, and 0.39 vs Ag/AgCl at pH = 4) also fall within this potential region. We can interpret these results to mean that a broad reversible wave experimentally observed at 0.32 V vs Ag/AgCl at pH = 4 (i) arises from an overall $4e^-/3H^+$ PCET processes for water activation to give bis-oxo intermediates. One reason for the positive deviations of computed potentials from the experimental value by about 0.3 V is that the actual heterogeneous reaction rate at the electrode−electrolyte interface depends on various surface effects, which are never covered by the isolated molecular system embedded in a homogeneous dielectric medium. Another reason is, of course, due to errors in DFT and PCM calculations.[37]

Even though the present results can explain qualitatively the origin of the experimentally observed broad reversible wave, there remains a question why μ-peroxo and μ-superoxo intermediates that would be electroactive [0.51−0.72 V vs SHE at pH = 0 (0.32−0.52 V vs Ag/AgCl at pH = 4)] at potentials where the oxidative activation of water is occurring [0.60−1.08 V vs SHE at pH = 0 (0.27−0.65 V vs Ag/AgCl at pH = 4)] cannot contribute to the broad reversible wave. To rationalize this point from a macroscopic standpoint, we considered a simple kinetic model that can illustrate its main features, as shown in Scheme 2, in which a rate constant, k_1, is assumed to be very small, and two competing parallel paths in the +2 and +4 systems are suppressed to simplify the complex analysis of behavior. After the steady state approximation is applied, the relation between the current density (j) and the electrode potential imposed by an outside source of voltage (E_{app}) would be derived from the Butler−Volmer equation for interfacial electron transfer, as expressed by eq 13, in which a_X is the activity of a species X, k_0 is a standard rate constant, and α is a transfer coefficient for the interfacial electron transfer.

Scheme 2

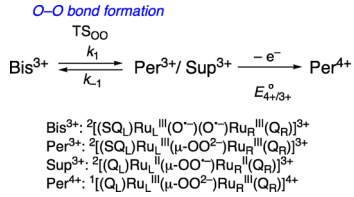

$$
\begin{aligned}
j &= Fk_0[a_{\mathrm{Per4+}} \exp\{-\alpha F(E_{app} - E^\circ_{4+/3+})/RT\} \\
&\quad - a_{\mathrm{Per3+/Sup3+}} \exp\{(1-\alpha)F(E_{app} - E^\circ_{4+/3+})/RT\}] \\
&= \frac{Fk_0}{k_{-1} + k_0 \exp\{(1-\alpha)F(E_{app} - E^\circ_{4+/3+})/RT\}} \\
&\quad [a_{\mathrm{Per4+}}k_{-1} \exp\{-\alpha F(E_{app} - E^\circ_{4+/3+})/RT\} - a_{\mathrm{Bis3+}}k_1 \\
&\quad \exp\{(1-\alpha)F(E_{app} - E^\circ_{4+/3+})/RT\}]
\end{aligned}
\tag{13}
$$

Using the standard free energies of activation for O−O bond making and breaking in an Arrhenius form, the necessary condition for anodic current flow ($j < 0$ A cm^{-2}) is given by eq 14.

$$
E_{app} > E^\circ_{4+/3+} + \Delta G^\circ_{OO}/F + (RT/F) \ln a_{\mathrm{Per4+}}/a_{\mathrm{Bis3+}} \tag{14}
$$

The third term associated with the activity dependence of potential is needed such that the kinetics equation reduces to the thermodynamic relation (the Nernst equation) in the limit of equilibrium, in which the net conversion rate is zero ($j = 0$ A cm^{-2}). The appearance of the second term means that the endothermicity for O−O formation causes a shift in the wave position in a positive direction by $\Delta G_{OO}{}^\circ/F$ (~0.40 V). On the other hand, slow kinetics on k_1 that decays exponentially with barrier height for O−O coupling ($\Delta G_{OO}{}^{\ddagger} \approx 20$ kcal mol^{-1}) will lower the relative contribution of the anodic component current (the second term in eq 13) sufficiently to prevent the electron transfer from occurring at a significant rate in the potential region where eq 14 would suggest that the reaction was possible. The activation energy needs to be supplied electrically to drive the reaction. Spin inversion between the ferro- and the antiferromagnetic pair of the bis-oxo intermediate, which is not addressed in this simple model, is an additional bottleneck for the actual reaction, giving rise to a further distortion in the shape of the oxidation wave. It follows from these considerations that we can discriminate clearly between the redox events preceding and following O−O bond formation by **1** in terms of the position and shape of the half-wave potential. The experimentally observed irreversible wave at 1.19 V vs Ag/AgCl at pH = 4 (ii) can, therefore, be taken as a sign of the occurrence of electron-transfer reaction after the TS$_{OO}$ for O−O coupling is passed. By interpreting so, we implicitly accept that the rate-determining transition state for water oxidation by **1** at pH = 4 is involved in the binding of a substrate water molecule, since more positive potentials (>1.5 V) are actually needed to drive the catalytic cycle at a certain rate (iii). Even though there is considerable uncertainty in computed values, this interpretation can be qualitatively understood by the fact that the open form of the superoxo complex is elevated above the closed form by >1.20 eV at pH = 0 (Figure 6) and >0.96 eV at pH = 4 (Figure S10, Supporting Information), in addition to the presence of a very high barrier

dx.doi.org/10.1021/ic402340d | Inorg. Chem. 2014, 53, 3973−3984

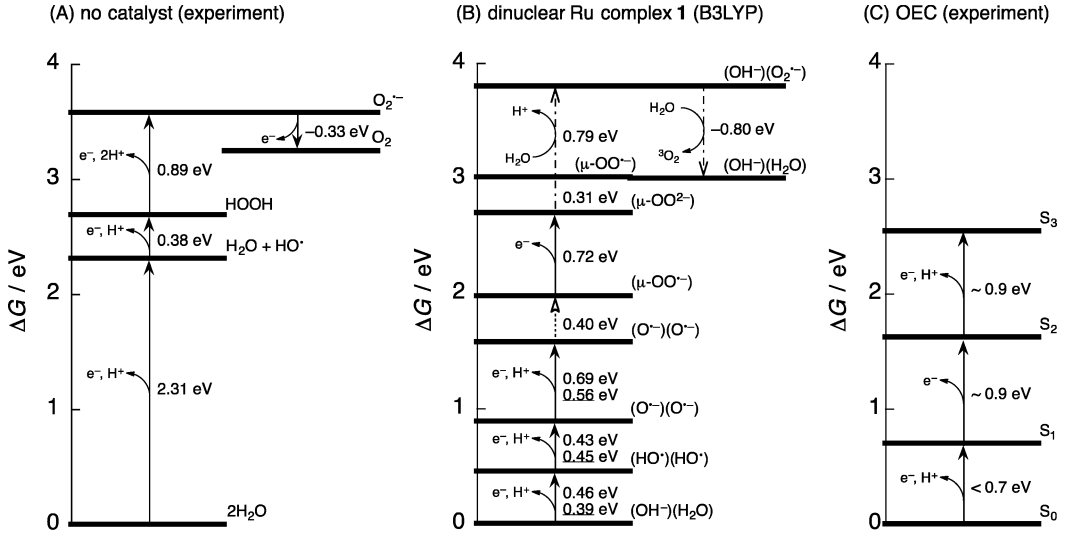

Figure 7. Energy diagrams for water oxidation at pH = 7 with reference to SHE in the absence (A) and presence of the catalyst **1** (B) in aqueous solution and in the OEC within the enzyme photosystem II (C); experimental data for cases A and C are taken from the literature;[2,38] computed data for case B are obtained at the B3LYP/BS2//BS1 level by the CPCM-UAKS method; results based on solution-phase geometries are underlined.[31]

of about 23−26 kcal mol^{-1} that has to be surmounted to invoke a dynamic movement of the catalyst linked to internal electron transfer (Figure S8E−G, Supporting Information).

Finally, we compared the energy diagrams for water oxidation at pH = 7 with reference to SHE in the absence (A) and presence of catalyst **1** (B) in aqueous solution and in the OEC within the enzyme photosystem II (C), as depicted in Figure 7; experimental data for cases A and C are taken from the literature.[2,38] If there is no catalyst (Figure 7A), the first one-electron oxidation of water to produce hydroxyl radical is thermodynamically very difficult (2.31 eV), although the second−fourth redox events following the initial one-electron oxidation are much easier (<0.89 eV) than the first. As a consequence, oxidation of water involves several high-energy intermediates, HO$^{\bullet}$, H_2O_2, $HO_2^{\bullet}$, and $O_2^{\bullet-}$, which are known as reactive oxygen species,[2] and a high overpotential arises from the inherent instability of free hydroxyl radical. Catalysis by the dinuclear Ru complex **1** prevents release of reactive oxygen species and causes a drastic change in the energy pattern, as shown in Figure 7B. Since the immediate electron donor of the catalyst **1** to the electrode is, in most cases, the semiquione ligand, all one-electron oxidation reactions fit into a relatively narrow energy range (0.39−0.72 eV), which is, however, too small to fulfill the thermodynamic requirement for the overall four-electron oxidation of water (E = 0.815 V vs SHE at pH = 7). The energy shortage is made up with large endothermicities for O−O bond formation and substrate incorporation, as shown by dashed arrows in Figure 7B, which result in bis-oxo intermediates that are much more difficult to oxidize than substrate waters bound to Ru sites. By applying a more positive potential, the sum of free energies for a μ-peroxo intermediate and for an electron on the electrode at the Fermi level is lowered to match the free energy of a bis-oxo intermediate, so that O−O bond formation becomes possible, as indicated in eq 14. This additional potential associated with chemical transformation gives rise to a high overpotential for water oxidation by **1**. An ideal situation is found in the redox behavior of the OEC in Figure 7C, in which sequential transitions in the S-state cycle operate at potentials reasonably close to the thermodynamic limit (E = 0.815 V); besides, they do not exceed the potential of a redox-active tyrosine residue $Tyr_Z^{\bullet+}/Tyr_Z$ (1.0−1.2 V), which acts as an electron-transfer mediator between the OEC and the chlorophyll complex P680.[6a]

4. CONCLUSIONS

The mechanism of electrocatalytic water oxidation by the dinuclear ruthenium complex containing redox-active quinone ligands **1** in aqueous solution has been studied by the hybrid DFT method. Substrate water binding at vacant coordination Ru sites is coupled with one or two proton loss, which allows pH-dependent variability in the proportion of different substrate-bound structures and following pathways for oxidative activation of the aqua/hydroxo ligands leading to formation of bis-oxo intermediates. In the presence of the quinone ligands, electrons originally on two substrate water molecules pass through these ligands in the intermediary stage to the electrode concurrently with loss of protons from the substrate ligands. This stepwise process involving the Q/SQ couple serves to control the range of redox potentials for interfacial electron transfer, although much still remains to be uncovered on electrode surface−catalyst interactions. The bis-oxo intermediates then undergo direct σ and π O−O coupling between two Ru(III)−O$^{\bullet}$ units with a significant barrier of about 20−35 kcal mol^{-1} and a large endothermicity of about 10−15 kcal mol^{-1}. The resulting μ-peroxo or μ-superoxo species can liberate oxygen with the need for the preceding binding of a substrate water molecule. Only after four-electron oxidation is completed can a water molecule bind to the complex with simultaneous loss of a proton. In this highly oxidized state, the anthracene moiety acts as a redox noninnocent ligand and undergoes long-range electron transfer with the reaction site, which sets in motion a large hinge-like bending of the catalyst required to open its compact, hydrophobic active site.

Two molecular transformations, O−O bond formation and hinge bending motion, are predicted to be thermodynamically and kinetically unfavorable processes, which prevent the electrocatalytic reaction from occurring at a significant rate, so that the electrode potential must be brought to considerably

dx.doi.org/10.1021/ic402340d | Inorg. Chem. 2014, 53, 3973−3984

positive values. The experimentally observed multistep electron-transfer behavior, which shows two resolved, anodic waves at 0.32 and 1.19 V vs Ag/AgCl before appreciable catalytic current flows (>1.5 V), is consistent with our interpretations that, despite the ability of the redox non-innocent quinone ligands to mediate efficient redox equilibrium between the substrate and the electrode, electron transfer following the endothermic O−O radical coupling requires an additional electrical work to form a O−O bond and thus is thermodynamically more difficult than the earlier steps in the catalytic cycle and that the magnitude of the catalytic current for water oxidation by **1** would be limited by the inherent sluggishness of the hinge bending motion of the μ-superoxo-bridged complex for incorporating a substrate water molecule.

■ ASSOCIATED CONTENT

Supporting Information

Thermodynamic results, geometrical parameters, natural orbitals, and energy diagrams; tables of thermodynamic results, diradical characters, and Mulliken charge and spin densities; Cartesian coordinates, absolute energies, and $\langle S \rangle^2$ values of optimized structures reported. This material is available free of charge via the Internet at http://pubs.acs.org.

■ AUTHOR INFORMATION

Corresponding Author

*E-mail: h-isobe@cc.okayama-u.ac.jp, isobe@chem.sci.osaka-u.ac.jp.

Notes

The authors declare no competing financial interest.

■ ACKNOWLEDGMENTS

This work was supported by a Grant-in-Aid for Specially Promoted Research (No. 24000018) from the Ministry of Education, Culture, Sports, Science and Technology (MEXT). Computations were carried out using Research Center for Computational Science, Okazaki, Japan.

■ REFERENCES

(1) (a) Lewis, N. S.; Nocera, D. G. *Proc. Natl. Acad. Sci. U.S.A.* **2006**, *103*, 15729−15735. (b) Balzani, V.; Credi, A.; Venturi, M. *ChemSusChem* **2008**, *1*, 26−58. (c) Walter, M. G.; Warren, E. L.; McKone, J. R.; Boettcher, S. W.; Mi, Q.; Santori, E. A.; Lewis, N. S. *Chem. Rev.* **2010**, *110*, 6446−6473. (d) Cook, T. R.; Dogutan, D. K.; Reece, S. Y.; Surendranath, Y.; Teets, T. S.; Nocera, D. G. *Chem. Rev.* **2010**, *110*, 6474−6502. (e) Concepcion, J. J.; House, R. L.; Papanikolas, J. M.; Meyer, T. J. *Proc. Natl. Acad. Sci. U.S.A.* **2012**, *109*, 15560−15564.

(2) Sawyer, D. T. *Oxygen Chemistry*; Oxford University Press: NewYork, 1991.

(3) (a) Rüttinger, W.; Dismukes, G. C. *Chem. Rev.* **1997**, *97*, 1−24. (b) Yagi, M.; Kaneko, M. *Chem. Rev.* **2001**, *101*, 21−35. (c) Dau, H.; Limberg, C.; Reier, T.; Risch, M.; Roggan, S.; Strasser, P. *ChemCatChem* **2010**, *2*, 724−761. (d) Lv, H.; Geletii, Y. V.; Zhao, C.; Vickers, J. W.; Zhu, G.; Luo, Z.; Song, J.; Lian, T.; Musaev, D. G.; Hill, C. L. *Chem. Soc. Rev.* **2012**, *41*, 7572−7589.

(4) Umena, Y.; Kawakami, K.; Shen, J.-R.; Kamiya, N. *Nature* **2011**, *473*, 55−60.

(5) In *Photosystem II: The Light Driven Water: Plastoquinone Oxidoreductase*; Wydrzynski, T. J., Satoh, K., Eds.; Springer: Dordrecht, The Netherlands, 2005.

(6) (a) McEvoy, J. P.; Brudvig, G. W. *Chem. Rev.* **2006**, *106*, 4455−4483. (b) Sauer, K.; Yano, J.; Yachandra, V. K. *Coord. Chem. Rev.* **2008**, *252*, 318−335. (c) Siegbahn, P. E. M. *J. Photochem. Photobiol. B* **2011**, *104*, 94−99. (d) Grundmeier, A.; Dau, H. *Biochim. Biophys. Acta* **2012**, *1817*, 88−105. (e) Cox, N.; Pantazis, D. A.; Neese, F.; Lubitz, W. *Acc. Chem. Res.* **2013**, *46*, 1588−1596.

(7) (a) Sun, L.; Hammarström, L.; Åkermark, B.; Styring, S. *Chem. Soc. Rev.* **2001**, *30*, 36−49. (b) Deng, Z.; Tseng, H.-W.; Zong, R.; Wang, D.; Thummel, R. *Inorg. Chem.* **2008**, *47*, 1835−1848. (c) Sala, X.; Romero, I.; Rodríguez, M.; Escriche, L.; Llobet, A. *Angew. Chem., Int. Ed.* **2009**, *48*, 2842−2852. (d) Concepcion, J. J.; Jurss, J. W.; Brennaman, M. K.; Hoertz, P. G.; Patrocinio, A. O. T.; Murakami Iha, N. Y.; Templeton, J. L.; Meyer, T. J. *Acc. Chem. Res.* **2009**, *42*, 1954−1965.

(8) (a) McDaniel, N. D; Coughlin, F. J.; Tinker, L. L.; Bernhard, S. *J. Am. Chem. Soc.* **2008**, *130*, 210−217. (b) Hull, J. F.; Balcells, D.; Blakemore, J. D.; Incarvito, C. D.; Eisenstein, O.; Brudvig, G. W.; Crabtree, R. H. *J. Am. Chem. Soc.* **2009**, *131*, 8730−8731.

(9) (a) Naruta, Y.; Sasayama, M.; Sasaki, T. *Angew. Chem., Int. Ed.* **1994**, *33*, 1839−1841. (b) Limburg, J.; Vrettos, J. S.; Liable-Sands, L. M.; Rheingold, A. L.; Crabtree, R. H.; Brudvig, G. W. *Science* **1999**, *283*, 1524−1527. (c) Mullins, C. S.; Pecoraro, V. L. *Coord. Chem. Rev.* **2008**, *252*, 416−443.

(10) (a) Yin, Q.; Tan, J. M.; Besson, C.; Geletii, Y. V.; Musaev, D. G.; Kuznetsov, A. E.; Luo, Z.; Hardcastle, K. I.; Hill, C. L. *Science* **2010**, *328*, 342−345. (b) Wasylenko, D. J.; Ganesamoorthy, C.; Borau-Garcia, J.; Berlinguette, C. P. *Chem. Commun.* **2011**, *47*, 4249−4251. (c) Dogutan, D. K.; McGuire, R., Jr.; Nocera, D. G. *J. Am. Chem. Soc.* **2011**, *133*, 9178−9180. (d) Artero, V.; Chavarot-Kerlidou, M.; Fontecave, M. *Angew. Chem., Int. Ed.* **2011**, *50*, 7238−7266.

(11) (a) Ellis, W. C.; McDaniel, N. D.; Bernhard, S.; Collins, T. J. *J. Am. Chem. Soc.* **2010**, *132*, 10990−10991. (b) Fillol, J. L.; Codolà, Z.; Garcia-Bosch, I.; Gómez, L.; Pla, J. J.; Costas, M. *Nat. Chem.* **2011**, *3*, 807−813.

(12) (a) Gersten, S. W.; Samuels, G. J.; Meyer, T. J. *J. Am. Chem. Soc.* **1982**, *104*, 4029−4030. (b) Gilbert, J. A.; Eggleston, D. S.; Murphy, W. R., Jr.; Geselowitz, D. A.; Gersten, S. W.; Hodgson, D. J.; Meyer, T. J. *J. Am. Chem. Soc.* **1985**, *107*, 3855−3864.

(13) Collins, J. P.; Sauvage, J. P. *Inorg. Chem.* **1986**, *25*, 135−141.

(14) (a) Lai, Y.-K.; Wong, K.-Y. *J. Electroanal. Chem.* **1995**, *380*, 193−200. (b) Rotzinger, F. P.; Munavalli, S.; Comte, P.; Hurst, J. K.; Gratzel, M.; Pern, F.-J.; Frank, A. J. *J. Am. Chem. Soc.* **1987**, *109*, 6619−6626. (c) Lebeau, E. L.; Adeyemi, S. A.; Meyer, T. J. *Inorg. Chem.* **1998**, *37*, 6476−6484.

(15) Llobet, A.; Curry, M. E.; Evans, H. T.; Meyer, T. J. *Inorg. Chem.* **1989**, *28*, 3131−3137.

(16) (a) Sens, C.; Romero, I.; Rodríguez, M.; Llobet, A.; Parella, T.; Benet-Buchholz, J. *J. Am. Chem. Soc.* **2004**, *126*, 7798−7799. (b) Zong, R.; Thummel, R. P. *J. Am. Chem. Soc.* **2005**, *127*, 12802−12803.

(17) (a) Concepcion, J. J.; Jurss, J. W.; Templeton, J. L.; Meyer, T. J. *J. Am. Chem. Soc.* **2008**, *130*, 16462. (b) Tseng, H.-W.; Zong, R.; Muckerman, J. T.; Thummel, R. *Inorg. Chem.* **2008**, *47*, 11763−11773. (c) Yoshida, M.; Masaoka, S.; Sakai, K. *Chem. Lett.* **2009**, *38*, 702−703. (d) Hetterscheid, D. G. H.; Reek, J. N. H. *Angew. Chem., Int. Ed.* **2012**, *51*, 9740−9747. (e) Wasylenko, D. J.; Palmer, R. D.; Berlinguette, C. P. *Chem. Commun.* **2013**, *49*, 218−227.

(18) (a) Sartorel, A.; Carraro, M.; Scorrano, G.; De Zorzi, R.; Geremia, S.; McDaniel, N. D.; Bernhard, S.; Bonchio, M. *J. Am. Chem. Soc.* **2008**, *130*, 5006−5007. (b) Geletii, Y. V.; Botar, B.; Kögerler, P.; Hillesheim, D. A.; Musaev, D. G.; Hill, C. L. *Angew. Chem., Int. Ed.* **2008**, *47*, 3896−3899. (c) Piccinin, S.; Sartorel, A.; Aquilanti, G.; Goldoni, A.; Bonchio, M.; Fabris, S. *Proc. Natl. Acad. Sci. U.S.A.* **2013**, *110*, 4917−1922.

(19) Tanaka, K.; Isobe, H.; Yamanaka, S.; Yamaguchi, K. *Proc. Natl. Acad. Sci. U.S.A.* **2012**, *109*, 15600−15605.

(20) (a) Wada, T.; Tsuge, K.; Tanaka, K. *Angew. Chem., Int. Ed.* **2000**, *39*, 1479−1482. (b) Wada, T.; Tsuge, K.; Tanaka, K. *Inorg. Chem.* **2001**, *40*, 329−337.

(21) Kobayashi, K.; Ohtsu, H.; Wada, T.; Kato, T.; Tanaka, K. *J. Am. Chem. Soc.* **2003**, *125*, 6729−6739.

(22) Muckerman, J. T; Polyansky, D. E.; Wada, T.; Tanaka, K.; Fujita, E. *Inorg. Chem.* **2008**, *47*, 1787−1802.

(23) (a) Ghosh, S.; Baik, M.-H. *Inorg. Chem.* **2011**, *50*, 5946−5957. (b) Ghosh, S.; Baik, M.-H. *Angew. Chem., Int. Ed.* **2012**, *51*, 1221−1224.
(24) Frisch, M. J.; Trucks, G. W.; Schlegel, H. B.; Scuseria, G. E.; Robb, M. A.; Cheeseman, J. R.; Scalmani, G.; Barone, V.; Mennucci, B.; Petersson, G. A.; Nakatsuji, H.; Caricato, M.; Li, X.; Hratchian, H. P.; Izmaylov, A. F.; Bloino, J.; Zheng, G.; Sonnenberg, J. L.; Hada, M.; Ehara, M.; Toyota, K.; Fukuda, R.; Hasegawa, J.; Ishida, M.; Nakajima, T.; Honda, Y.; Kitao, O.; Nakai, H.; Vreven, T.; Montgomery, J. A., Jr.; Peralta, J. E.; Ogliaro, F.; Bearpark, M.; Heyd, J. J.; Brothers, E.; Kudin, K. N.; Staroverov, V. N.; Kobayashi, R.; Normand, J.; Raghavachari, K.; Rendell, A.; Burant, J. C.; Iyengar, S. S.; Tomasi, J.; Cossi, M.; Rega, N.; Millam, J. M.; Klene, M.; Knox, J. E.; Cross, J. B.; Bakken, V.; Adamo, C.; Jaramillo, J.; Gomperts, R.; Stratmann, R. E.; Yazyev, O.; Austin, A. J.; Cammi, R.; Pomelli, C.; Ochterski, J. W.; Martin, R. L.; Morokuma, K.; Zakrzewski, V. G.; Voth, G. A.; Salvador, P.; Dannenberg, J. J.; Dapprich, S.; Daniels, A. D.; Farkas, Ö.; Foresman, J. B.; Ortiz, J. V.; Cioslowski, J.; Fox, D. J. *Gaussian 09*, Revision C.01; Gaussian, Inc.: Wallingford, CT, 2010.
(25) (a) Becke, A. D. *Phys. Rev. A* **1988**, *38*, 3098−3100. (b) Lee, C.; Yang, W.; Parr, R. G. *Phys. Rev. B* **1988**, *37*, 785−789. (c) Becke, A. D. *J. Chem. Phys.* **1993**, *98*, 5648−5652.
(26) (a) Hay, P. J.; Wadt, W. R. *J. Chem. Phys.* **1985**, *82*, 270−283. (b) Hehre, W. J.; Radom, L.; Schleyer, P. v. R.; Pople, J. A. *Ab Initio Molecular Orbital Theory*; Wiley: New York, 1986. (c) Roy, L. E.; Hay, P. J.; Martin, R. L. *J. Chem. Theory Comput.* **2008**, *4*, 1029−1031.
(27) (a) Barone, V.; Cossi, M. *J. Phys. Chem. A* **1998**, *102*, 1995−2001. (b) Cossi, M.; Rega, N.; Scalmani, G.; Barone, V. *J. Comput. Chem.* **2003**, *24*, 669−681.
(28) Camaioni, D. M.; Schwerdtfeger, C. A. *J. Phys. Chem. A* **2005**, *109*, 10795−10797.
(29) Lim, C.; Bashford, D.; Karplus, M. *J. Phys. Chem.* **1991**, *95*, 5610−5620.
(30) Reiss, H.; Heller, A. *J. Phys. Chem.* **1985**, *89*, 4207−4213.
(31) During research, we found that six intermediates, $^{3}[(Q_L)Ru_L^{III}(OH)(OH)Ru_R^{III}(Q_R)]^{4+}$, $^{4}[(Q_L)Ru_L^{III}(O^{\bullet-})(OH)Ru_R^{III}(Q_R)]^{4+}$, $^{4}[(SQ_L)Ru_L^{III}(O^{\bullet-})(O^{\bullet-})Ru_R^{III}(Q_R)]^{3+}$, $^{5}[(Q_L)Ru_L^{III}(O^{\bullet-})(O^{\bullet-})Ru_R^{III}(Q_R)]^{4+}$, $^{2}[(SQ_L)Ru_L^{III}(O^{\bullet-})(O^{\bullet-})Ru_R^{III}(Q_R)]^{3+}$, and $^{1}[(Q_L)Ru_L^{III}(O^{\bullet-})(O^{\bullet-})Ru_R^{III}(Q_R)]^{4+}$, have a very long O···O interatomic distance (5.6−7.9 Å, Figure S3, Supporting Information) in the gas phase, which is denoted "far" in ref 22; however, after reoptimizations were done in water, all these "far" geometries converged to compact structures with a short O···O interatomic distance (3.3−3.8 Å, Figure S3, Supporting Information), called "near" in ref 22. In the main text of this article, we report various thermodynamic properties based on "near" (solution-phase) geometries, which are underlined in the figures. The use of "far" geometries affects redox potentials by less than 0.2 V and pK_a values by less than 3. The presence of "near" and solvent-accessible "far" geometries that are similar in energy and interconvertible may have implications for proton exchange necessary for PCET reactions, since the permanently "near" geometry cannot readily release protons from the aqua/hydroxo ligands with no external hydrogen bond.
(32) (a) Huynh, M. H. V.; Meyer, T. J. *Chem. Rev.* **2007**, *107*, 5004−5064. (b) Warren, J. J.; Tronic, T. A.; Mayer, J. M. *Chem. Rev.* **2010**, *110*, 6961−7001. (c) Weinberg, D. R.; Gagliardi, C. J.; Hull, J. F.; Murphy, C. F.; Kent, C. A.; Westlake, B. C; Paul, A.; Ess, D. H.; McCafferty, D. G.; Meyer, T. J. *Chem. Rev.* **2012**, *112*, 4016−4093.
(33) Koper, M. T. M. *Chem. Sci.* **2013**, *4*, 2710−2723.
(34) In $^{4}[(SQ_L)Ru_L^{III}(O^{\bullet-})(O^{\bullet-})Ru_R^{III}(Q_R)]^{3+}$, an unpaired electron in the ligands is actually delocalized into both Q_L and Q_R, leading to a symmetric electronic structure described as $^{4}[(Q_L^{-0.5})Ru_L^{III}(O^{\bullet-})(O^{\bullet-})Ru_R^{III}(Q_R^{-0.5})]^{3+}$ (Table S1, Supporting Information); however, geometry reoptimization with solvent correction included[31] results in an asymmetric electronic structure, $^{4}[(SQ_L)Ru_L^{III}(O^{\bullet-})(O^{\bullet-})Ru_R^{III}(Q_R)]^{3+}$, in which an unpaired electron in the ligands is essentially localized on one semiquinone ligand, SQ_L (Table S1, Supporting Information). Therefore, just because the bis-oxo intermediate has an unusual electronic structure at the gas-phase geometry like $^{4}[(Q_L^{-0.5})Ru_L^{III}(O^{\bullet-})(O^{\bullet-})Ru_R^{III}(Q_R^{-0.5})]^{3+}$, it does not follow that we can rule out a possibility of O−O bond formation in $^{4}[(SQ_L)Ru_L^{III}(O^{\bullet-})(O^{\bullet-})Ru_R^{III}(Q_R)]^{3+}$.[23b]
(35) The energetic argument for the hinge bending motion in the gas phase depends on long-range and dispersion corrections, which are neglected in B3LYP calculations (Figure S8, Supporting Information); more discussion is given in the Supporting Information.
(36) (a) Prabhakar, R.; Siegbahn, P. E. M.; Minaev, B. F.; Ågren, H. *J. Phys. Chem. B* **2002**, *106*, 3742−3750. (b) Isobe, H.; Yamanaka, S.; Kuramitsu, S.; Yamaguchi, K. *J. Am. Chem. Soc.* **2008**, *130*, 132−149.
(37) (a) Yang, X.; Baik, M.-H. *J. Am. Chem. Soc.* **2004**, *126*, 13222−13223. (b) Tsai, M.-K.; Rochford, J.; Polyansky, D. E.; Wada, T.; Tanaka, K.; Fujita, E.; Muckerman, J. T. *Inorg. Chem.* **2009**, *48*, 4372−4383.
(38) Vass, I.; Styring, S. *Biochemistry* **1991**, *30*, 830−839.